Abstract 1

Thermal Diffusivity Imaging of CFRP: Spatial Correlation Between Lock-in Thermography-Based Measurement and Synchrotron X-ray CT Simulation on Identical Region †

Ryohei Fujita [1],*, Song Boxi [1] and Hosei Nagano [1]

[1] Department of Mechanical Engineering, Nagoya University, Foro-cho, Chikusa-ku, Nagoya-shi 464-8603, Japan; nagano@mech.nagoya-u.ac.jp
* Correspondence: fujita.ryouhei.w7@f.mail.nagoya-u.ac.jp;
† Presented at the 18th International Workshop on Advanced Infrared Technology and Applications, Kobe, Japan, 15–19 September 2025.

1. Introduction

With the increasing adoption of wide-bandgap semiconductors such as SiC and GaN in high-power electronics, the thermal management of semiconductor devices has become critical. High thermal conductivity thermal interface materials (TIMs) are essential to minimize thermal contact resistance. While advanced fillers such as graphene, diamond nanosheets, and hexagonal boron nitride (h-BN) have been proposed, their effectiveness strongly depends on the spatial continuity and orientation of the filler network. Excessive filler loading, on the other hand, degrades mechanical strength and flexibility. Visualizing the spatial distribution of thermal conductivity is thus essential to optimize the filler structure. This study examines the correlation between the spatial distribution of thermal diffusivity and the internal filler structure in composite materials, employing both experimental and numerical methods. We proposed and have been developing the lock-in thermography-based laser periodic heating method to obtain the spatial thermal diffusivity distribution of composites[1]. In this study, the internal fiber-resin structure of CFRP (carbon fiber reinforced plastic) specimens was visualized using synchrotron X-ray computed tomography (SR-CT), meshed using GeoDict, and used to perform transient heat conduction simulations in ANSYS Fluent. The thermal diffusivity distribution obtained from simulations was compared with that measured by the lock-in thermography method.

2. Methods

2.1. Materials and Simulation

The CFRP laminate plate used for the measurement was fabricated from T700SC/#2592 prepreg with a $[0/90_3]s$ stacking sequence. The sample size was $10 \times 4 \times t1.176$ mm, as shown in Fig. 1(a). The out-of-plane thermal diffusivity D distribution of this specimen was evaluated. SR-CT was performed at the BL8S2 beamline of the Aichi Synchrotron Radiation Center in Japan. The observation area was a 1.3×1.3 mm region of the specimen as shown in Fig. 1(b). To visualize the microstructure of carbon fibers with a diameter of 7 μm, a high-resolution optical system with a spatial resolution of 0.65 μm was employed. SR-CT data reconstructed from the X-ray transmission images were binarized using the simulation software GeoDict. To prevent misidentification of voids as carbon fibers, the FiberFind module was utilized to extract the axial coordinates of the carbon

fibers, enabling reconstruction of fiber regions. As a result, the reconstructed model from SR-CT successfully replicated the actual structure, including fiber-fiber contacts and fiber-resin interfaces. However, components other than fibers and resin, such as voids, were excluded, which is a future work in the image segmentation process. To perform thermal conduction simulations, a segment containing the full CFRP laminate structure was extracted from the SR-CT data as shown in Fig. 1(c). Mesh generation compatible with AN-SYS Fluent was then performed for finite element analysis. The final computational model consisted of 250 × 250 × 1850 voxels as shown in Fig. 1(d). Unsteady-state heat conduction simulations were conducted using the implicit Euler method, based on the thermal property summarized in Table 1. The boundary conditions included sinusoidal thermal input at the surface, with adiabatic conditions applied to the sides and rear surface. The voxel size was 0.65 μm, the heating frequency was 1 Hz, the time step was 0.01 s, and the simulation was run for three cycles with a convergence criterion of residuals less than 1×10^{-10}. Lock-in analysis was applied to the 2D temperature-time history at the surface opposite to the heated side, yielding a distribution of phase delays to the input heat wave. This phase delay distribution was then converted to D using Eq. 4.
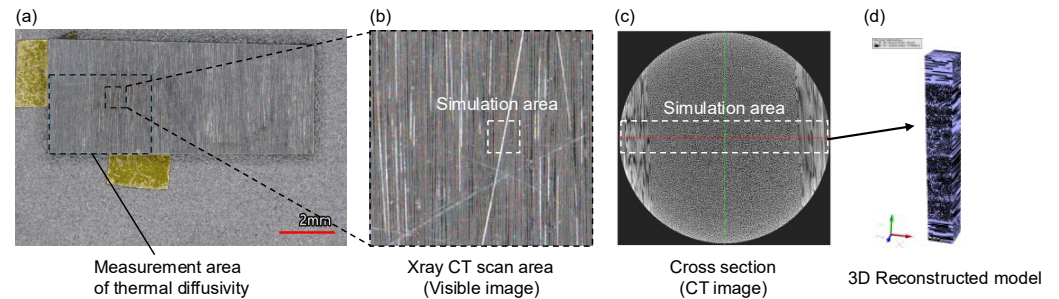
Figure 1. (**a**) CFRP sample and measurement area of thermal diffusivity. (**b**) SR-CT scan area on CFRP sample. (**c**) Cross-sectional image of reconstructed SR-CT image. (**d**) 3D reconstructed image.

Table 1. Thermophysical properties for numerical simulation.

Material	Epoxy resin	Carbon fiber
Thermal conductivity (W/mK)	0.21 [2]	9.60 (Longitudinal) [3] 2.73 (Transverse) [4]
Specific heat capacity (J/gK)	1331 [2]	752 [3]
Density (kg/m³)	1160 [2]	1800 [3]
Thermal contact resistance (m²K/W)	1×10⁻⁶ (CF-Resin, Interlaminar)	

2.2. Measurement Principle

To evaluate the distribution of the effective D in the out-of-plane direction of the specimen, a 1-D quasi-steady-state heat conduction model is introduced. When the surface of the specimen is uniformly subjected to periodic rectangular wave heating at a frequency *f*, and the rear surface is thermally insulated, the temperature response of the specimen can be expressed as follows[1]:

$$\tilde{T}(t,d) = \frac{q}{\lambda \pi \sigma \sinh(\sigma d)} \cdot e^{i\omega t - \pi/2}. \qquad (1)$$

where $\tilde{T}$ is the AC temperature, Q_0 is the input heat rate per unit area, λ is the thermal conductivity, $\sigma = \sqrt{i\omega/D}$, $\omega\ (= 2\pi f)$ is the angular frequency, and d is the thickness of the specimen. Since $\tilde{T}$ oscillates at the same harmonics of q, then amplitude A and phase ϕ at $z = d$ are shown as follows:

$$A = \left|\tilde{T}(t,d)\right|, \quad \phi = \tan^{-1}[\tilde{T}(t,d)]. \qquad (2)$$

The phase distribution acquired from the infrared camera's detector array is measured in the frequency domain and converted into a D distribution through the fitting of Eq.2.

When calculating D from numerical simulation results, frequency-domain analysis imposes a high computational cost. In cases where the heating frequency is sufficiently high ($\sigma d \to \infty$), Eq. 1 can be simplified as follows.

$$\lim_{f \to \infty}\left[\tilde{T}(t,d)\right] = \frac{q}{\lambda\pi\sqrt{2\pi f/D}} \cdot e^{-kd+i(2\pi ft-3\pi/4-kd)} \,. \tag{3}$$

The phase delay is given by $\phi_\infty = -3\pi/4 - kd$, where $k = \sqrt{\pi f/D}$ is referred to as the wavenumber. D is obtained as follows:

$$D = \pi f d^2/(3\pi/4 + \phi_\infty)^2 \,. \tag{4}$$

By using Eq. 4, D can be determined from the phase delay at a single frequency, thereby reducing computational cost. However, in actual measurements, the absolute phase includes system-induced delays; therefore, Eq. 4 is applied to the numerical simulation only.

2.3. Measurement Setup and Condition

The measurement apparatus is illustrated in Fig. 2. The measurements were conducted using a cooled-type thermography camera (InfReC H9000, Japan Avionics) equipped with a 5X microscopic lens, which achieved a spatial resolution of 5 μm. The temperature response was processed using a digital lock-in process, allowing acquisition of the phase delay distribution. The semiconductor LASER beam was applied through a square-core multimode fiber and uniformly heated onto the surface. To minimize heat loss, the entire specimen was measured under a vacuum condition. The heating frequency ranged from 0.2 to 0.4 Hz, the laser power was set to 2500 mW, and the lock-in integration time corresponded to 120 cycles.
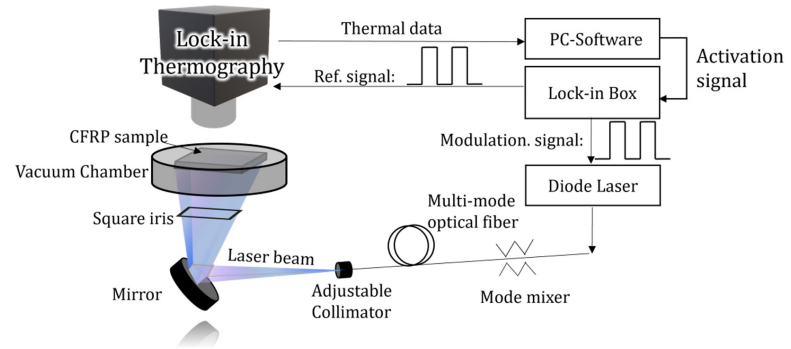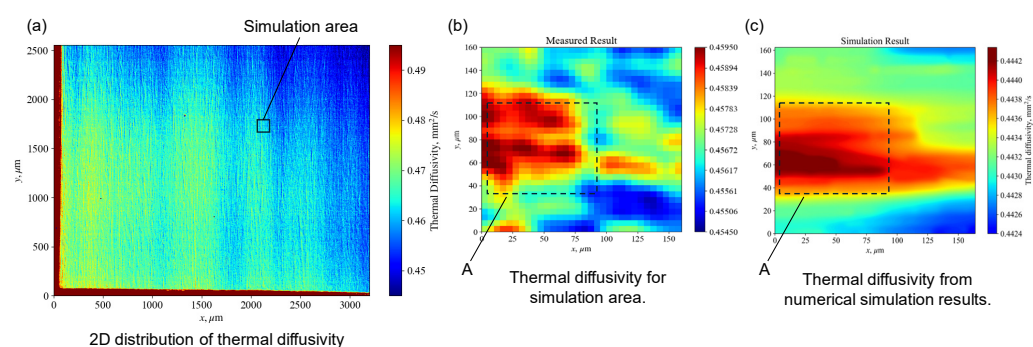

Figure 2. Measurement apparatus.

3. Results and Discussion

Fig. 3(a) shows the measured D distribution. A striped pattern with alternating high and low values along the X-axis direction is observed. This trend was also confirmed in previous macroscale measurements of CFRP laminates[5]. The average D in the measured region was 0.457 mm²/s, which is in good agreement with the reported value[5]. An enlarged view of the same region used in the simulation is presented in Fig. 3(b). Based on the reconstructed CFRP model obtained from SR-CT, numerical simulation yielded the D distribution shown in Fig. 3(c). The simulation and experimental results show a similar trend, particularly in region A. However, some differences are observed in another region. In CFRP laminates, the 0° plies near the front and back surfaces can become parallel to the X-ray beam direction depending on the rotation angle. As a result, X-ray transmission intensity becomes lower for the 0° layers than for the 90° layers. This leads to a relatively high level of noise in the fiber structure of the 0° layers. Such image degradation is considered to contribute to the differences observed in the D distributions. The average D obtained from the simulation was 0.443 mm²/s, with a difference of approximately 2.8% from the experimental result, demonstrating good agreement in absolute values.

(a) Simulation area — 2D distribution of thermal diffusivity
(b) Measured Result — Thermal diffusivity for simulation area.
(c) Simulation Result — Thermal diffusivity from numerical simulation results.

Figure 3. (**a**) Thermal diffusivity distribution from the measurement. (**b**) Simulation area of measurement results. (**c**) Simulation results from SR-CT reconstructed CFRP model.

4. Conclusions

The thermal diffusivity distribution obtained by measurement was compared with that derived from heat conduction simulations based on synchrotron SR-CT at the same region of the CFRP specimen. A consistent trend was observed between the measured and simulated distributions. However, challenges remain in accurately modeling the fiber structure, and some differences in local distribution were identified. Future work will aim for full agreement between simulation and measurement, and further investigation will be conducted to clarify the correlation between the structural features and the factors contributing to the observed distribution. This approach offers valuable insights into the structural design of composite materials with enhanced thermal conductivity.

References

1. Alasli, A. et al. Thermophysical Properties Mapping of Composites by Lock-in Thermography: Applications on Carbon Fiber Reinforced Plastics. Int. J. Thermophys. 2022, 43, doi:10.1007/s10765-022-03109-7.
2. Harada, M. et al. Thermal and Mechanical Properties of Tetra-Functional Mesogenic Type Epoxy Resin Cured with Aromatic Amine. *J. Appl. Polym. Sci.* **2018**, *135*, 46181, doi:10.1002/app.46181.
3. T700S Technical Data Sheet, Available online: https://toray-cfe.com/wp-content/uploads/2025/02/Torayca-T700S-Technical-Data-Sheet.pdf (accessed on 05 June 2025).
4. Ji, X. et al. Anisotropic Thermal and Electrical Conductivities of Individual Polyacrylonitrile-Based Carbon Fibers. *Carbon N. Y.* **2022**, *197*, 1–9, doi:10.1016/j.carbon.2022.06.005.
5. Fujita, R. et al. Lock-in Thermographic Measurement and Model-Based Evaluation of Effective Thermal Diffusivity to Quantify Early Stage Fatigue Damage of CFRP. In Proceedings of the Thermosense: Thermal Infrared Applications XLV; SPIE, June 12 2023; Vol. 12536, pp. 65–70.